Validation of the Computation of Rocket Nozzle Admittances with Linearized Euler Equations

R. Kathan⋆, D. Morgenweck⋆, R. Kaess⋆⋆ and T. Sattelmayer⋆
⋆Lehrstuhl für Thermodynamik, Technische Universität München
Boltzmannstraße 15, D-85748 Garching
⋆⋆Astrium GmbH, Space Transportation, TP 24
81663 München, Germany

Abstract

High pressure fluctuations coupled with unsteady heat release can affect a rocket engine seriously. Especially when the oscillations match higher eigenmodes such as T1, T1L1 and T2, T2L1, the pressure amplitude can reach a critical level. This paper deals with the investigation of the nozzle admittance, which is an important value to characterize the influence of the nozzle on the pressure inside the combustion chamber. Two different nozzle geometries are investigated experimentally at high frequencies. A method to decouple the acoustic modes is presented. The results are compared against an existing theory and simulated data.

1. Nomenclature

Latin symbols

c	$[m/s]$	Speed of sound
D	$[m]$	Diameter
f	$[1/s]$	Frequency
F	$[m/s]$	Downstream wave
G	$[m/s]$	Upstream wave
k	$[1/m]$	Wave number
L	$[m]$	Length
m	$[-]$	m-th transverse Mode
$\dot{m}$	$[kg/s]$	Massflow
n	$[-]$	n-th root of $\partial J_m/\partial r$
p	$[Pa]$	Pressure
r	$[m]$	Radial coordinate
R	$[m]$	Radius
s	$[-]$	Root of $\partial J_m/\partial r$
t	$[s]$	Time
u	$[m]$	Axial velocity
x	$[m]$	Axial coordinate
Y	$[m^2 s/kg]$	Admittance
$\mathscr{Y}$	$[-]$	Nondim. Admittance ($\mathscr{Y} = Y\bar{\rho}\bar{c}$)

Greek symbols

α	$[^\circ]$	Angle
δ	$[^\circ]$	Angle
ρ	$[kg/m^3]$	Density
ω	$[1/s]$	Angular frequency ($\omega = 2\pi f$)
θ	$[^\circ]$	Azimuthal coordinate
κ	$[-]$	Wave number ratio

Head pointer

$\bar{a}$	Mean value
$\hat{a}$	Complex amplitude
a'	Fluctuation
$\vec{a}$	Vector

Indices

C	Combustion chamber
A	Nozzle A
B	Nozzle B
i	Sensor number
T	Nozzle throat
O	Nozzle outlet
r	Radial direction
Ref	Reference sensor or surface
x	Axial direction
$+$	Positive direction
$-$	Negative direction
θ	Azimuthal direction

Superscripted symbols

0	Modeclass T0LR0
1	Modeclass T1LR0
2	Modeclass T2LR0

Mathematic operators and functions

i		Imaginary unit ($i^2 = -1$)
J_m		Besselfunction first kind of order m
∇	$\left(\frac{\partial}{\partial x}, \frac{\partial}{\partial y}, \frac{\partial}{\partial z}\right)$	Differential operator
exp		Exponential function
$\Re$		Real part
$\Im$		Imaginary part

Nondimensional numbers

M	u/c	Mach number

2. Introduction

One of the major challenges in the development of rocket engines is the prediction of combustion instabilities. They are a result of high pressure fluctuations coupled with unsteady heat release [6]. Under certain conditions this phenomenon can affect the combustion chamber tremendously, resulting in a complete failure of the engine. Consequently the acoustic pressure fluctuations inside the combustion chamber have to be known. Especially when high frequency oscillations match higher eigenmodes such as T1, T1L1 and T2, T2L1, the pressure amplitude can reach a critical level. Therefore, these modes have to be considered. Beside the combustion chamber, liners and faceplate, the main component that affects the pressure inside the engine is the nozzle.

The Lehrstuhl für Thermodynamik at the Technische Universität München performs research activities in the field of acoustics. Different test facilities and numerical tools are used for the investigations of rocket engines and stationary gas turbines with the aim of getting a better understanding of the physical processes yielding to combustion instabilities. The focus is on the investigation of new design rules for future engines in terms of stability predictions. One of the main fields of the experimental research is the validation of numerical simulations and the allocation of adequate boundary conditions. The admittance is an appropriate parameter to describe the acoustics of a passive element such as a nozzle. Since the wave propagation is known for duct elements like a cylindrical combustion chamber, the admittance can be calculated with the impedance tube method. Previous investigations showed a dependency of the admittance on the frequency and the shape of the corresponding eigenmodes. The admittance is a qualitative value for stability predictions. A negative real part of the admittance can destabilize the rocket engine [1] [9] [7].

To validate numerically computed nozzle admittances, measurements were undertaken. The presented test facility is operated under cold conditions with pressurized air and consists of a nozzle and a cylindrical combustion chamber. It can be excited at specific frequencies by a siren. Two different types of nozzles are used. The first nozzle (A) represents a scaled geometry of a real engine. The second one (B) represents a generic geometry of an engine design that is used to conserve the flow field characteristics of the real engine. The chamber is equipped with sensors in axial and circumferential direction to provide dynamic pressure signals. The one-dimensional impedance tube method considers the homogeneous axial mean flow in the chamber and provides the nozzle admittance for different modes. It is extended to consider the first (T1, T1L1,...) and the second transverse (T2, T2L1,...) modes.

The experimental results are used to validate the one-dimensional Linearized Euler Equation (LEE) tool provided by Bell and Zinn [9]. Furthermore, the results are compared with the three-dimensional LEE tool PIANO-SAT.

3. Theory

Rocket chambers usually consist of a cylinder and an attached nozzle. Since the length and the diameter of the cylinder are very often of similar size, a purely one-dimensional approach is improper. Instead, the three dimensional wave field has to be considered.
The pressure and the axial velocity can be written as the sum of a mean and a fluctuation value

$$p = \bar{p} + p' \tag{1}$$

$$u = \bar{u} + u' \tag{2}$$

Considering only harmonic oscillations, the pressure fluctuations can be rewritten as an infinite sum of normal modes [2]

$$p' = \sum_{k=1}^{\infty} \hat{p}_k exp\left(i\omega t\right) \Psi_k \tag{3}$$

which leads to the Helmholtz equation [2]

$$-\frac{\omega^2}{c^2}\Psi_k - \nabla^2\Psi_k = 0 \tag{4}$$

A solution for typical rocket geometries can be found by a separation approach and a transformation into cylindrical coordinates.

$$\Psi_k = X_k\left(x\right) R_k\left(r\right) \Theta_k\left(\theta\right) \tag{5}$$

These three functions describe the mode shape in the appropriate direction. The solutions in radial and transverse directions for a hard cylinder wall can be easily found in the literature [5]. In axial direction the mean flow is considered in the up- and downstream wavenumber. By introducing an up- (G) and downstream (F) wave, the axial solution can be found. Table 1 gives an overview on the functions and the corresponding wave numbers as a function of the principal wave number $k = \omega/c$. Since the highest frequency is $4000Hz$ and modes with higher cut-on frequencies [8]

Table 1: Characteristic functions and wave numbers

Direction	**Function**	**Wave number**
Radial	$R_k = J_m\left(k_r^{mn} r\right)$	$k_r^{mn} = s^{mn}/R$
Transverse	$\Theta_k = cos\left(k_\theta^{mn}\theta + \delta^m\right)$	$k_\theta^{mn} = m$
Axial	$X_k = \bar{\rho}\bar{c}\left[F^{mn} exp\left(-ik_{x+}^{mn}x\right) + G^{mn} exp\left(-ik_{x-}^{mn}x\right)\right]$	$k_{x+}^{mn} = \frac{k}{1-M^2}\left(-M + \sqrt{1-\left(\frac{k_r^{mn}}{k}\right)^2\left(1-M^2\right)}\right)$
		$k_{x-}^{mn} = \frac{k}{1-M^2}\left(-M - \sqrt{1-\left(\frac{k_r^{mn}}{k}\right)^2\left(1-M^2\right)}\right)$

Table 2: Cut-on frequencies for different modes

	Mode-class	**m**	**n**	**Form**	$\mathbf{s^{mn}}$	**Cut-on frequencies**	
						Nozzle A	**Nozzle B**
Longitudinal	0	0	0	L1, L2,...	0	-	-
1. Radial	0R1	0	1	R1, R1L1, R1T1,...	3.8318	4322 Hz	4306 Hz
2. Radial	0R2	0	2	R2, R2L1, R2T1,...	7.0155	7914 Hz	7883 Hz
1. Transverse	1	1	1	T1, T1L1, T1R1,...	1.8412	2077 Hz	2069 Hz
2. Transverse	2	2	1	T2, T2L1, T2R1,...	3.0541	3445 Hz	3432 Hz

cannot propagate, only pure longitudinal (T0LR0), the first (T1LR0) and second (T2LR0) transverse mode classes are considered. Table 2 gives an overview on the cut-on frequencies for frequencies below $4306Hz$. It is more convenient to neglect the superscripted index n since it is always equal to zero ore one in this case. The complex pressure and velocity amplitude can be written into

$$\hat{p} = \hat{p}^0 + \hat{p}^1 + \hat{p}^2 \tag{6}$$

$$\hat{u} = \hat{u}^0 + \hat{u}^1 + \hat{u}^2 \tag{7}$$

with the following expressions (8 - 13) at the cylinder surface ($r = R_C$).

$$\hat{p}^0 = \bar{\rho}\bar{c}\left[F^0 exp\left(-ik_{x+}^0 x\right) + G^0 exp\left(-ik_{x-}^0 x\right)\right] J_0\left(s^0\right) \tag{8}$$

$$\hat{p}^1 = \bar{\rho}\bar{c}\left[F^1 exp\left(-ik_{x+}^1 x\right) + G^1 exp\left(-ik_{x-}^1 x\right)\right] J_1\left(s^1\right) cos\left(1\theta + \delta^1\right) \tag{9}$$

$$\hat{p}^2 = \bar{\rho}\bar{c}\left[F^2 exp\left(-ik_{x+}^2 x\right) + G^2 exp\left(-ik_{x-}^2 x\right)\right] J_2\left(s^2\right) cos\left(2\theta + \delta^2\right) \tag{10}$$

$$\hat{u}^0 = \left[\kappa_+^0 F^0 exp\left(-ik_{x+}^0 x\right) - \kappa_-^0 G^0 exp\left(-ik_{x-}^0 x\right)\right] J_0\left(s^0\right) \quad (11)$$

$$\hat{u}^1 = \left[\kappa_+^1 F^1 exp\left(-ik_{x+}^1 x\right) - \kappa_-^1 G^1 exp\left(-ik_{x-}^1 x\right)\right] J_1\left(s^1\right) cos\left(1\theta + \delta^1\right) \quad (12)$$

$$\hat{u}^2 = \left[\kappa_+^2 F^2 exp\left(-ik_{x+}^2 x\right) - \kappa_-^2 G^2 exp\left(-ik_{x-}^2 x\right)\right] J_2\left(s^2\right) cos\left(2\theta + \delta^2\right) \quad (13)$$

$\kappa_\pm^m = k_{x\pm}^m / \left(k - Mk_{x\pm}^m\right)$ represents a correction factor to achieve the axial velocity component. To compute the pressure and velocity, the up- (F^m) and downstream (G^m) waves and the correction angles (δ^m) have to be known. This can be achieved by solving the linear equations[1]

$$\hat{p}_i - \left[\hat{p}^0 + \hat{p}^1 + \hat{p}^2\right] \rightarrow min \quad (14)$$

where $\hat{p}_i$ are the measured pressure values. Since one pressure sensor provides one complex value (or amplitude and phase), at least eight sensors are necessary. Finally the admittance can be calculated at any position inside the cylindrical combustion chamber for each mode class

$$Y^m = \frac{\hat{u}^m}{\hat{p}^m} \quad (15)$$

4. Experimental setup

The measurements were performed at the Lehrstuhl für Thermodynamik. The experiment consists of a cylindrical part and an attached nozzle. Two different nozzles were used in this investigation. Instead of an injector faceplate, a perforated plate is used to homogenize the incoming flow. The experiment is operated with pressurized air without combustion. The air is provided by a high pressure feed system with several mass flow control units. An overview of the test facility in the two different configurations is given in figure 1. The geometries of the nozzles have been selected such that they are fully specified using the few geometry parameters of the nozzle available in the admittance calculation code developed by Bell and Zinn [9].

The nozzle geometry is shown in figure 2 with the appropriate values provided in table 3. Both nozzles consist of a subsonic and a supersonic part to make sure that the flow is accelerated through the nozzle throat from subsonic to supersonic velocities to ensure sonic conditions in the nozzle throat. An external siren excites the chamber at specific frequencies up to $5600Hz$ and is connected sidewise (nozzle A) and coaxial (nozzle B) to the cylindrical combustion chamber. The shape of the siren outlet is adapted such that it provides almost perfect smooth sinusoidal pulses.

The cylindrical combustion chamber has several ports in axial as well as in circumferential direction and can be equipped with dynamic pressure sensors[2]. 32 sensors were used in the configuration of nozzle A while their number was reduced to 13 for nozzle B. The analog signals were simultaneously sampled[3] at $2^{15}Hz$ for one second of measurement time. Afterwards, they were Fourier transformed to provide amplitude and phase at the corresponding excitation frequency. For each excitation frequency, several recordings were acquired to obtain a representative time average of the acoustic pressure in amplitude and phase.

[1] The linear equation system was solved with a Levenberg-Marquardt algorithm

[2] PCB Piezotronics, model M106B: Internally protected against mechanical vibrations, uses a high pass filter to suppress the mean pressure.

[3] A/D data acquisition unit: National Instruments NI PXI-4472

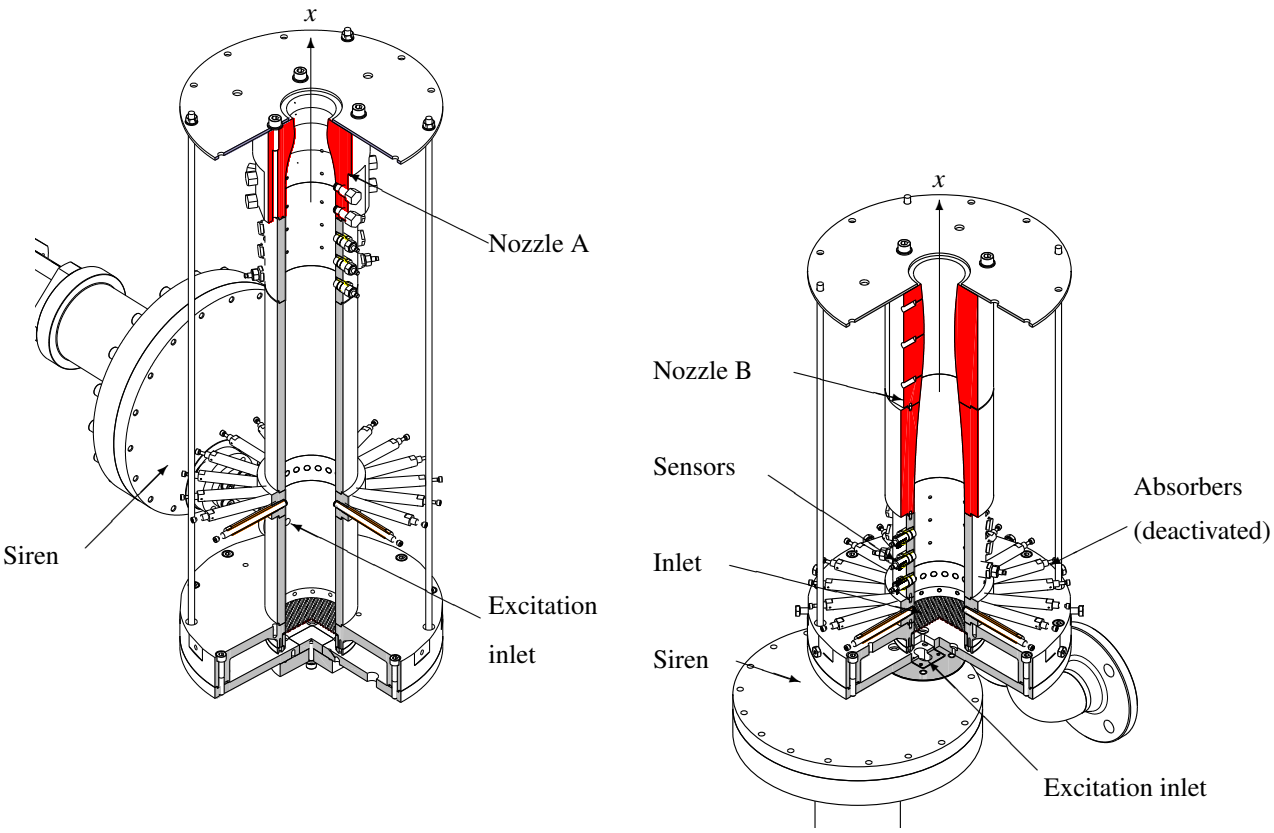

Figure 1: Nozzle A (left) and B (right)

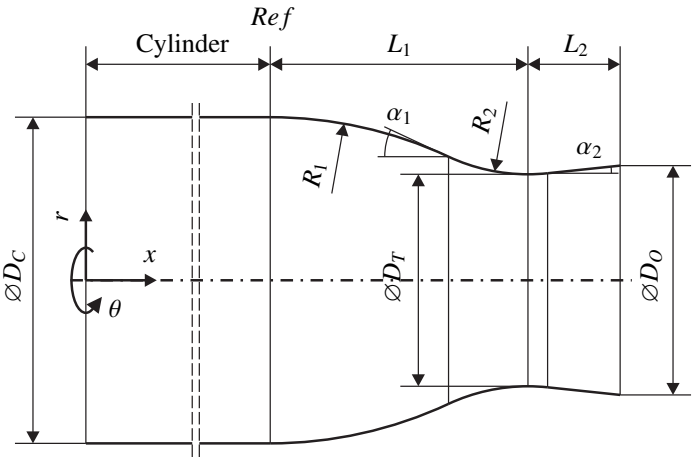

Figure 2: Nozzle contour

Symbol	Nozzle A	Nozzle B	Unit
$\varnothing D_C$	92	92	mm
$\varnothing D_T$	60	56	mm
$\varnothing D_O$	64	67	mm
R_1	119	1469	mm
R_2	53	544	mm
L_1	73	273	mm
L_2	25	81	mm
α_1	25	7	°
α_2	6	6	°
p	1.654	1.664	bar
$\dot{m}$	1.150	1.000	kg/s
M	0.25	0.22	–

Table 3: Geometry values of nozzle A and B

5. Available data

The experimental results are compared by two available sets of data:

- Simulated results by Kaess et. al. [4]
- Numerical solution provided by Bell and Zinn [9]

5.1 Simulated results

The admittance of the nozzle was computed with the 3D simulation tool PIANO-SAT [3] [4] [6] based on the Linearized Euler Equations (LEE). The available admittance data are simulated for a frequency close to the cut-on frequency of mode class 1 for nozzle A.

5.2 Numerical solution

Bell and Zinn [9] provide numerical results in comparison to the theory developed by Crocco [2] for the admittances of choked nozzles that considers three dimensional flow oscillations including higher modes. By specifying the mode class, this method provides the corresponding admittance.

6. Results

The experiments presented in this section have been performed for a frequency range from $1000Hz$ to $4000Hz$ (nozzle A) and $3000Hz$ (nozzle B) with a step size of $10Hz$. Figure 3 shows the pressure amplitude of one typical sensor as a

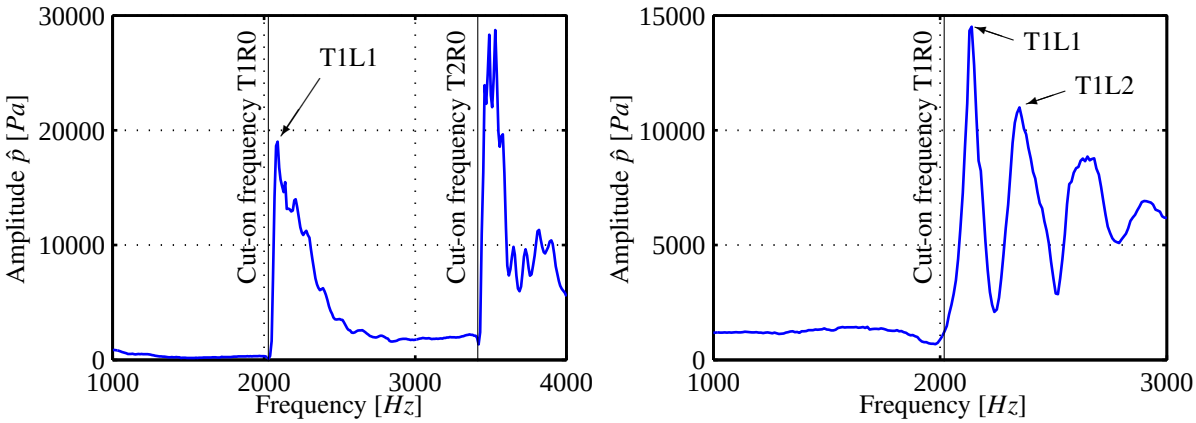

Figure 3: Typical overall pressure of one sensor, nozzle A (left) and nozzle B (right)

function of the excitation frequency for both configurations. Below the cut-on frequency of mode class 1, the values are very small. It can be recognized that the amplitudes at the calculated cut-on frequency which is valid for a pure T1 mode are low as well. Therefore, a pure T1 mode cannot propagate in both investigated configurations. The reason for that is, that the up- and downstream boundary of the cylindrical combustion chamber do not behave like a solid wall and hence induce an axial pressure gradient which changes the mode shape into a T1L1 mode. Short above the theoretical cut-on frequency, the amplitude increases by a factor of 20 for nozzle A and 10 for nozzle B.

First the quality of the reconstructed values is analyzed. Figure 4 shows the pressure measured by two different sensors for the two configurations compared to the reconstructed values following equation 6. They are in nearly perfect agreement with each other over the whole frequency range.

Figure 5 shows the measured admittance compared to the results provided by the theory from Bell and Zinn for mode

classes 0, 1 and 2 in terms of real and imaginary part and the simulated results for mode class 1. It can be recognized that the values of mode class 0 and 1 match quite well below the cut-on frequency of the next higher mode class. Above, some deviations can be recognized. A reason for that could be, that the pressure amplitude of one mode class is very small compared to the one from the next higher mode class (see figure 3), assuming the same scale of amplitude short below and above the cut-on frequency of the lower mode class. Since the admittance is the ratio of the velocity fluctuation to the pressure fluctuation, its value can get quite imprecise due to small pressure values in the denominator. Nevertheless, this is irrelevant, because the overall pressure is dominated by the next higher mode.

Short above the cut-on frequency, where the pressure amplitudes are high, theory and experiment match quite well. This frequency region is relevant for further stability analysis, since the real part of the admittance is negative and in consequence could change the damping behavior significantly.

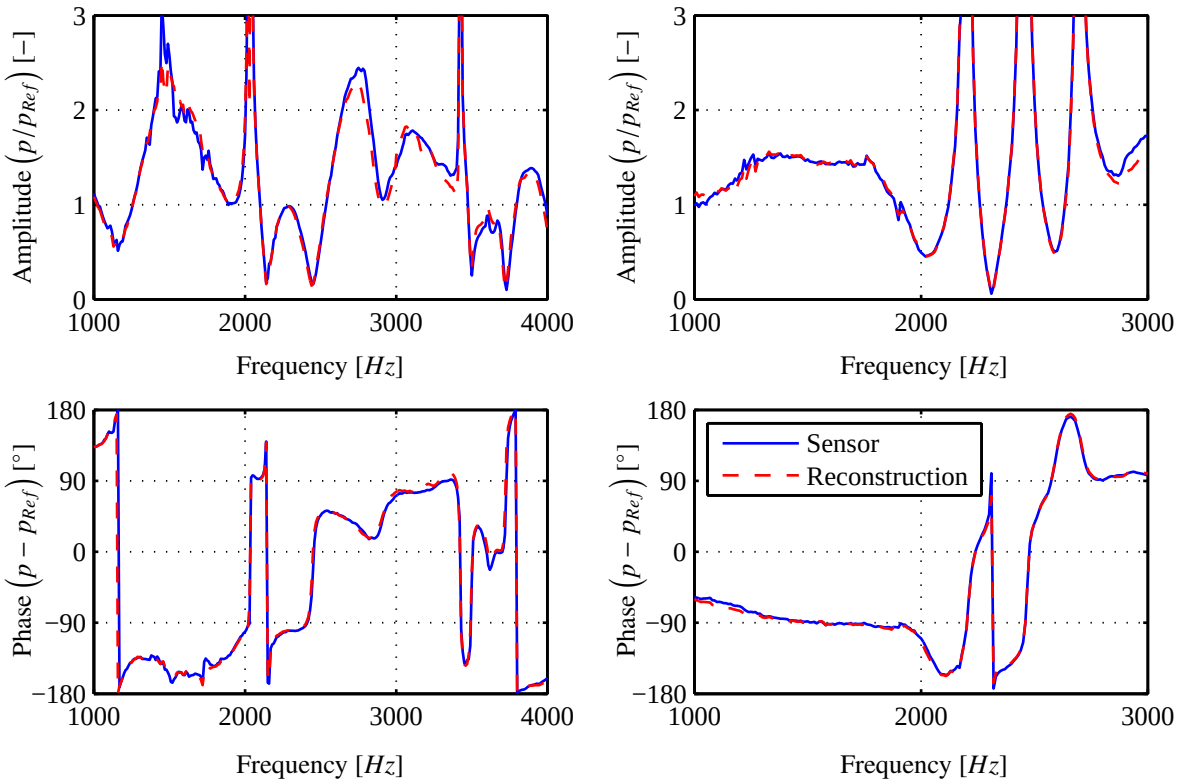

Figure 4: Measured and reconstructed pressure data of one sensor, nozzle A (left) and nozzle B (right)

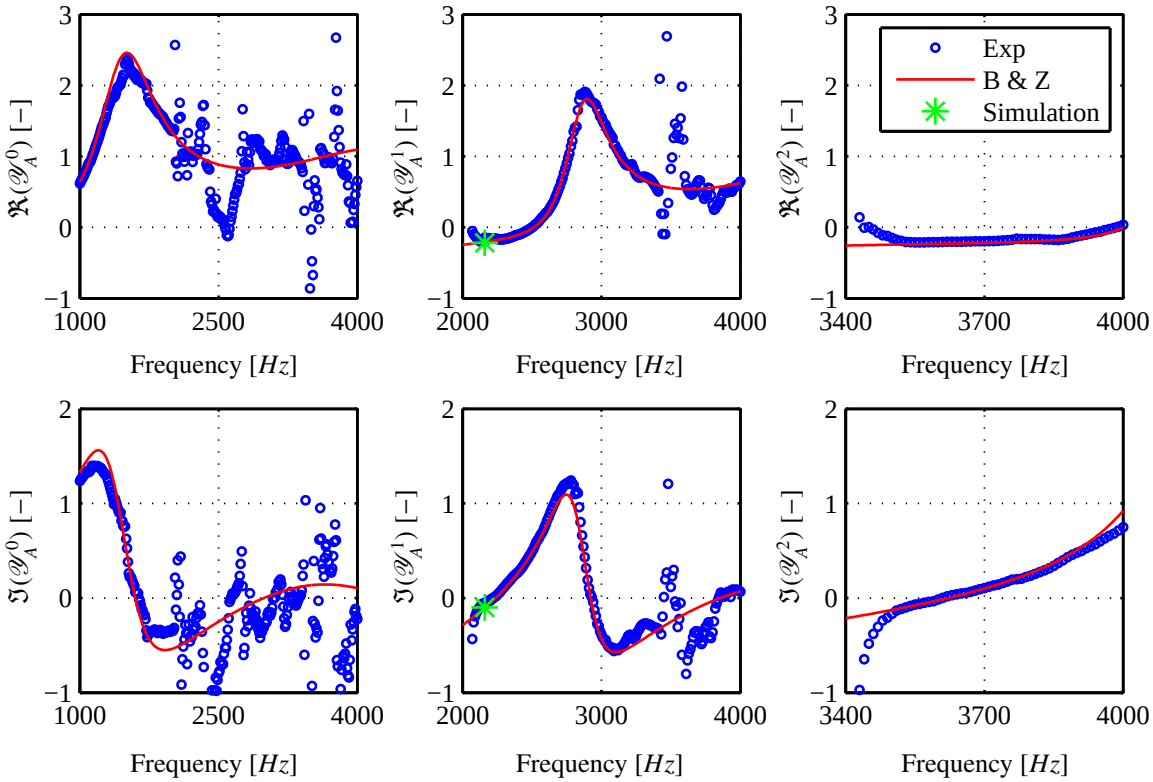

Figure 5: Admittances of nozzle A (mode 0 and mode 1)

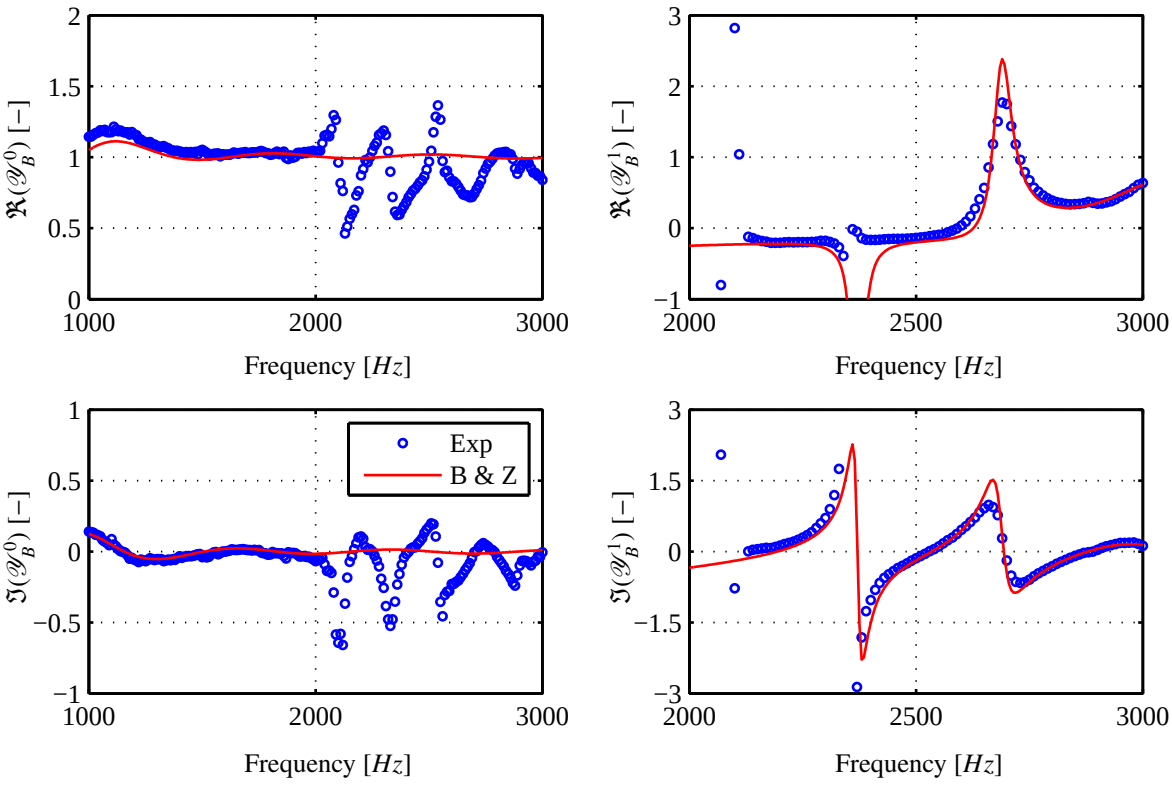

Figure 6: Admittances of nozzle B (mode 0 and mode 1)

7. Conclusion

The real and imaginary parts of the admittance are in very good agreement with the theoretical values. For all investigated mode classes and nozzles, it can be easily seen, that the values of the real and imaginary part of the admittance are equal to the computed values based on the theory provided by Bell and Zinn for almost every frequency. At some frequencies minor differences occur. The simulated results are also in good agreement with the experimental results. For mode class 0 the absolute values of the real and the imaginary part of the experimental results are marginally below the theory for the whole frequency range. This yields lower damping. For mode class 1 it can be concluded that the simulated values and the theory of Bell and Zinn can be confirmed. The experiment delivers the same negative real part of the nozzle admittance for specific frequencies which corresponds to a destabilizing effect.

8. Acknowledgements

This project was supported by Astrium GmbH, Space Transportation and Prof. Dr.-Ing. Jan Delfs from the Institute of Aerodynamics and Flow Technology at the German Aerospace Research Center (DLR) who provided PIANO. Their support is gratefully acknowledged.

References

[1] Bell, W. A.: *Experimental Determination of Threedimensional Liquid Rocket Nozzle Admittances*, Georgia Institute of Technology Atlanta, Diss., 1972

[2] Crocco, L. ; Sirignano, W. A.: Stability of Three-Dimensional Motions in a Combustion Chmber / North Atlantic Treaty Organisation. 1967 (AGARDograph 117). – Forschungsbericht

[3] Delfs, J. W. ; Grogger, H. A. ; Lauke, T. G. W.: Numerical simulation of aeroacoustic noise by DLR's aeroacoustic code PIANO / DLR Braunschweig. 2002. – Forschungsbericht

[4] Kaess, R. ; Koeglmeier, S. ; Schmid, M. ; Sattelmayer, T. : Linearized Euler Calculation of Acoustics of a Rocket Combustion Chamber / 2nd REST Modelling Workshop. Ottobrunn, October 2010. – Proceedings

[5] Morse, P. ; Ingard, K. : *Theoretical Acoustics*. Princeton University Press, 1968. – 927 S. – None

[6] Pieringer, J. ; Sattelmayer, T. ; Fassl, F. : Simulation of Combustion Instabilities in Liquid Rocket Engines with Acoustic Perturbation Equations. In: *Journal of Propulsion and Power* 25 (2009), September-October, Nr. 5

[7] Pieringer, J. E.: *Simulation Selbsterregter Verbrennungsschwingungen in Raketenschubkammern im Zeitbereich*, Technische Universität München, Institut für Energietechnik, Lehrstuhl für Thermodynamik, Diss., 2008

[8] Rienstra, S. W. ; Hirschberg, A. ; Rienstra, S. W. (Hrsg.) ; Hirschberg, A. (Hrsg.): *An Introduction to Acoustics*. Eindhoven University of Technology, 2010

[9] Zinn, B. T. ; Bell, W. A. ; Daniel, B. R. ; Smith Jr., A. J.: Experimental Determination of Three-Dimensional Liquid Rocket Nozzle Admittances. In: *AIAA* 11 (1973), Nr. 11